184

Jordanian Journal of Computers and Information Technology (JJCIT), Vol. 11, No. 02, June 2025.

TOWARDS OPTIMIZING THE DOWNLINK TRANSMIT POWER IN UAV-INTEGRATED IRS WIRELESS SYSTEMS

Ali Reda, Tamer Mekkawy and Ashraf Mahran

ABSTRACT

Air-to-ground interference poses a critical challenge in integrating unmanned aerial vehicles (UAVs) into cellular networks. In downlink scenarios, UAVs can withstand significant interference from co-channel base stations (BSs) due to the guaranteed line-of-sight (LoS) link with ground users. Our research focuses on power optimization in BSs and applying green-energy principles to pave the way for more sustainable and energy-efficient BSs within UAV-integrated wireless systems. To this end, this paper investigates a downlink UAV communication scenario in which the intelligent reflecting surface (IRS) is mounted on the UAV to practically nullify the interference originating from the co-channel BSs. We formulate the IRS beamforming matrix to reduce transmit power by optimizing passive beamforming for IRS elements, incorporating adjustments to phase shifts and amplitude coefficients while considering the positioning of the UAV. The proposed optimization problem is non-convex and thus a successive convex-approximation (SCA) method is adopted to convert all constraints into a quadratic approximation. Simulation results demonstrate that the proposed SCA algorithm provides an efficient transmit-power minimization approach with low computational complexity for large IRS, since it achieves close-to-optimal performance and significantly outperforms conventional systems without IRS. In interference scenarios and with different numbers of IRS meta-atoms, the proposed algorithm achieves a power reduction of approximately 8 and 13 dBm, while maintaining the same required signal-to-interference-plus-noise ratio.

KEYWORDS

1. INTRODUCTION

Unmanned aerial vehicles (UAVs) have become a critical enabler for delivering wireless *ad-hoc* connectivity, especially in disaster areas and harsh environments [1]. However, because line-of-sight (LoS) transmission is dominant in aeronautical communication, UAVs are frequently affected by signal interference from terrestrial networks. On the other hand, intelligent reflecting surface (IRS) has emerged recently as a practical way to enhance the wireless-propagation environment by improving communication and coverage performance [2]. An IRS is made up of several passive meta-atoms that are coordinated by a microcontroller in order to create a directional reflection of the incident signal towards a desirable direction. The reflected signals are added either constructively or destructively to the received signal to strengthen or weaken the signal-to-interference-plus-noise ratio (SINR) by carefully tweaking the phase shifts. For systems beyond the fifth generation (5G), IRS-assisted wireless networks have demonstrated considerable spectral and power efficiency [3]. IRS-assisted UAV enables intelligent reflection over the air. Compared to terrestrial IRS set-ups, IRS-supported UAV systems are more effective at establishing robust LoS connections with ground BSs due to the UAV's elevated position, consequently reducing signal blockage [4].

The next-generation wireless networks are poised to transform wireless communication, facilitating the realization of advanced applications, like holographic telepresence, autonomous vehicles and pervasive sensing. However, future networks will require higher data rates, reduced latency and highly reliable, secure communications to support these innovations. This demand will require the deployment of additional BSs and network components, resulting in heightened energy consumption [5]. The cooperative-RSMA system with IRS assistance has proven to reduce the system's energy consumption [6]. Consequently, it is imperative to explore potential energy-saving opportunities within the next generation. One crucial area of focus involves optimizing the phase-shift configurations of multiple IRS meta-atoms to achieve the desired signal amplification or interference

A. Reda, T. Mekkawy and A. Mahran are with the Avionics Department, Military Technical College, Cairo 11331, Egypt. Emails: ali.aboelyazeed@ieee.org, mekkawy@ieee.org and a.mahran@ieee.org

suppression in IRS-assisted systems. However, it is computationally demanding to solve the joint optimization of the passive beamforming at the IRS and the active beamforming at the BS directly due to its non-convex nature. Some algorithms based on alternating optimization (AO) [7], semi-definite relaxation (SDR) [8] and manifold optimization [9] maximize the performance of passive IRS beamforming. Consequently, the aforementioned approaches necessitate many iterations or significant computing complexity to reach convergence for large IRS elements. IRS applications have garnered significant attention for enhancing the quality of both uplink and downlink transmissions. A joint transmit beamforming of the access point (AP) and the passive reflection of the IRS was frequently discussed in technical literature. More specifically, in [10], the authors maximized the secrecy rate of the communication link with a single eavesdropper in a multi-input-single-output (MISO) system. In [11], the authors utilized the transmit beamforming and the reflecting coefficients to maximize the weighted sum secrecy rate. Additionally, the authors in [12] studied the secure-communication capabilities of the IRS-assisted multi-user in a MISO interference channel. We use the best active transmit beamforming strategy along with passive phase shifts for the IRSs in this work. These are found using SDR and successive convex approximation (SCA) methods. The passive-beamforming capabilities of IRSs were used to attain an optimal performance balance between terrestrial aerial users and UAVs in [13].

The authors in [14] investigated the security and spectrum-efficiency aspects of secondary users in Cognitive Radio Networks (CRNs) with the assistance of the IRS. Specifically, they studied the implementation of the IRS in an underlay CRN and co-designed the transmit and reflect beamforming vectors at the IRS. To address the challenge of maximizing secrecy capacity in communication systems, they proposed an iterative AO algorithm. In [15], the authors introduced the IRS and utilized an AO approach to maximize the secrecy rate in Multiple-Input Multiple-Output (MIMO) wiretap channels. Jiang et al. investigated the use of IRS in MIMO cognitive radio systems in [16]. To solve the sum-rate maximization problem, they introduced the weighted minimal mean square error (WMMSE) approach and an AO-based method. The authors in [17] addressed the problem of optimizing the beampattern for an eavesdropping target in an IRS-aided integrated sensing and communication (ISAC) system. They employed an SCA algorithm to jointly optimize the transmit beamforming of the AP and the phase-shift matrix of the IRS, aiming to maximize the beampattern gain.

1.1 Related Work

The selection of a phase shifter poses a challenge in IRS-aided communication systems [18]. Previous works on IRS generally assume that each reflecting unit functions as a continuous phase shifter, enabling the phase-shift matrix to adjust for reflective beamforming [19]-[20]. The authors in [8] introduced the joint active and passive-beamforming problem, utilizing the SDR method to minimize transmit power at the BS. However, implementing this approach in practice is challenging due to hardware limitations. Conversely, in [21], the authors investigated IRS-aided wireless networks assuming that only a discrete number of phase shifts are deployed at each reflecting unit. Furthermore, the utilization of non-orthogonal multiple access (NOMA) in conventional multi-IRS downlink systems is investigated in [22], where the authors presented a successive phase-rotation approach to determine the phase shifts sequentially.

In recent years, several papers have focused on IRS-assisted wireless communication [23]. A significant challenge in this system is the joint optimization of phase shifts at the IRS and beamforming vectors at the BS. In [24], a study was conducted on a massive multiple-input multiple-output communication system, where the problem of maximizing the minimum signal-to-interference-plus-noise ratio was addressed. This was achieved by jointly optimizing the signal power, transmit precoding vector and the effective phase shifts at the large intelligent surface. Additionally, optimizing both the active beamforming at the BS and the passive beamforming at the IRS can minimize the BS transmit power to meet mobile-user rate requirements [8]. Users can flexibly modify the channel conditions at the IRS, introducing an additional degree of freedom (DoF) to enhance system performance. In [25], a power-minimization framework was explored within an IRS-enabled NOMA network. The optimization of transmit beamforming and IRS phase shifts was addressed and solved using an alternating optimization approach. The authors in [26] addressed the problem of minimizing power consumption in a downlink-communication scenario assisted by the IRS. This optimization

186

Jordanian Journal of Computers and Information Technology (JJCIT), Vol. 11, No. 02, June 2025.

aimed to satisfy minimum SINR thresholds. This paper takes a joint approach, considering both power control and IRS reflection coefficients in the optimization process. On the other hand, the UAV-assisted IRS can significantly improve communication-system reliability and overcome obstacles by adjusting both its position and phase shifts. For instance, in [27], the authors explored the concept of a UAV-carried IRS, aiming to minimize the average total-power consumption of the system through joint optimization of the UAV's trajectory/velocity and the IRS's phase shifts. In [28], the authors investigated a joint active and passive-beamforming approach using a generalized Bender's decomposition-based algorithm. This approach utilizes codebook-based passive beamforming across multiple IRS in a multi-user MISO system. The primary objective is to minimize the transmit power while optimizing the system performance. Moreover, the authors in [29] utilized the SCA and SDR techniques to address the non-convex transmit beamforming-optimization problem. Their objective was to maximize the energy efficiency of a multi-user MISO system aided by IRS.

Unlike terrestrial wireless channels, which often suffer from significant path loss and multi-path effects, the elevated position of UAVs typically provides more dominant LoS channels, leading to improved communication performance. However, these strong LoS links also make UAVs more vulnerable to attacks from terrestrial nodes, such as eavesdropping and jamming [30]. IRS-assisted UAVs offer several advantages, including the ability to dynamically adjust the IRS's position through UAV maneuvering. This introduces a new degree of freedom for IRS optimization. Moreover, mounting the IRS on the UAV enables full- angle reflection and increases the number of LoS links [31]. Numerous studies have focused on optimizing transmit power in IRS-assisted UAV systems [32].

1.2 Motivation and Contributions

Compared to traditional, fixed-insert IRS-aided transmission, the benefits of combining the IRS with a UAV are clear. But, there is a lack of research; therefore, further study is required. Our suggested technique has lower per-iteration complexity compared to [8], which is mostly caused by the system's reliance on SDR to solve the optimization problem. The use of AO in [7] makes the problem easier to understand, but the solution that comes out might not be very good because of how the design factors are interdependent. Furthermore, convergence of a penalty-based strategy necessitates a large number of iterations. In this study, we look at how IRS-aided UAVs deal with the problem of balancing transmit power and quality-of-service (QoS) needs in downlink communication. This paper introduces a powerful optimization approach that ensures solution convergence by combining SCA and second- order cone-programming (SOCP) techniques. By breaking the original problem into manageable convex sub-problems with closed-form solutions, the suggested SCA method effectively handles the non-convexity of the original problem. This is achieved by utilizing linear approximations and convex lower limits. Monte Carlo simulations show that the low-complexity SCA achieves efficient performance, far better than benchmark schemes, evaluating the usefulness of this method. Finally, the following are the technical contributions of our paper:

- SCA is adopted to counterbalance the non-convex characteristic of the optimization problem, aiming to minimize the transmit power by optimizing the reflection coefficients of the IRS meta-atoms. This optimization guarantees the fulfillment of both QoS and minimum power for a specific SINR value. By formulating the problem as a SOCP, all optimization variables are updated simultaneously in each iteration. This approach guarantees the algorithm's provable convergence.

- We report an interference-mitigation scheme that utilizes a single UAV equipped with an IRS, eliminating the need for deploying multiple IRSs near each ground BS [13]. This approach effectively addresses interference issues between UAV and ground users during the UAV's downlink communications. The IRS-aided UAV employs passive beamforming to mitigate the interference originating from the co-channel BSs.

- The problem is formulated as a SOCP and the convergence is shown by updating the variables simultaneously. Moreover, the algorithm successfully reduces the power consumption by around 13 dBm, while maintaining the required SINR level.

The paper is structured as follows: Section 2 presents the system model and formulates the optimization problem. In Section 3, we decompose the power optimization and passive beamforming

using the SCA algorithm. Section 4 summarizes the convergence and complexity analysis. Section 5 shows the numerical results obtained. Finally, the conclusions are summarized in Section 6.

Notations

Regular and bold small letters stand for scalars and vectors, while bold capital letters are used for matrices. The magnitude of a scalar x is represented by $|x|$, while the Euclidean norm of a vector $\boldsymbol{x}$ is denoted as $\|\boldsymbol{x}\|$. The transpose of the matrix $\mathbf{X}$ is represented by $\mathbf{X}^{\mathrm{T}}$, the conjugate transpose by $\mathbf{X}^{\mathrm{H}}$ and the rank is $\mathrm{rank}(\mathbf{X})$. The notation $\mathrm{diag}(\mathbf{X})$ refers to a diagonal matrix. The notation $\mathbb{C}^{m \times n}$ represents the set of $m \times n$ complex matrices. Complex numbers' real and imaginary parts are presented as $\Re(\cdot)$ and $\Im(\cdot)$, respectively. Finally, the letter $\boldsymbol{j}$ represents the imaginary unit $\sqrt{-1}$.
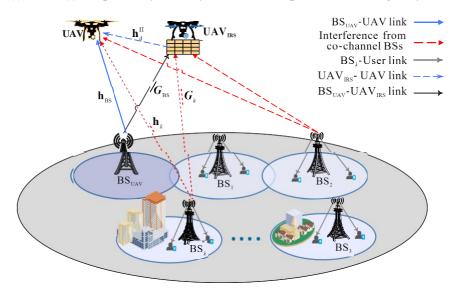

Figure 1. Downlink interference in a cellular-UAV scenario.

2. SYSTEM MODEL AND PROBLEM DEFINITION

This section introduces the system model under consideration and analyzes the functionality of the IRS modules in minimizing the required transmit power.

2.1 System Model

We investigate a downlink cellular-connected UAV scenario, assuming all BSs have N_r antennas and a UAV is connected directly with $\mathrm{BS_{UAV}}$. This scenario includes K additional co-channel BSs serving ground UEs, introducing potential interference for the UAV. In contrast to conventional terrestrial inter-cell interference (ICI), cellular-connected UAV results in an interference problem that includes aerial-ground interference; *i.e.*, interference resulting from co-channel terrestrial BSs and inter-UAV interference; *i.e.*, interference resulting among co-channel UAVs. An aided integrating UAV with IRS, $\mathrm{UAV_{IRS}}$, is deployed to minimize the interference that is caused in the kth BS, BS_k, $\forall k \in \mathcal{S} = \{1,2,\ldots,K\}$. Here, we assume that only aerial-ground interference exists, as shown in Fig. 1. Let $\mathrm{UAV_{IRS}}$ have fixed altitude and elevation angle and the IRS has N meta-atoms.

The meta-atoms in $\mathrm{UAV_{IRS}}$ aim to enhance the power efficiency of the communication link between the $\mathrm{BS_{UAV}}$ and the UAV. We assume that the amplitude, $\alpha_i \in [0,1]$ and the phase, $\theta_i \in [0,2\pi)$, $\forall i \in \{1,2,\ldots,N\}$, can be independently adjusted for each meta-atom. While the phase and amplitude responses of the meta-atom are physically interconnected, there exist design approaches that effectively mitigate this inter-dependency [33]. Consequently, we denote the reflection diagonal matrix associated with the IRS as:

$$\boldsymbol{\Theta} = \mathrm{diag}\begin{bmatrix} \alpha_1 e^{j\theta_1} & \alpha_2 e^{j\theta_2} & \ldots & \alpha_N e^{j\theta_N} \end{bmatrix}, \in \mathbb{C}^{N \times N} \tag{1}$$

The BSs are positioned at the Cartesian coordinates $(x_{\mathrm{BS},k}, y_{\mathrm{BS},k}, h_{\mathrm{BS},k})$, while the coordinates of the UAV-IRS are $(x_{\mathrm{U}}, y_{\mathrm{U}}, h_{\mathrm{U}})$, which are assigned during the time interval. In this scheme, it is assumed that the UAV and the $\mathrm{UAV_{IRS}}$ operate as a swarm system, with the UAV maintained at a fixed altitude,

h_{UAV} and at a close distance with a defined flight period T and maximum speed $V_{\max}$.

Given that the UAV operates at a sufficient altitude, we assume that the link between the UAV and the BS is only LoS, as described in [34]. Additionally, we assume that a single antenna is installed on the UAV. Let h_{BS} and $\mathbf{h}_k \in \mathbb{C}^{1 \times N_r}$ be the direct channel from BS_{UAV} to UAV and the interfering channel from BS_k to UAV, respectively, while the channel from IRS to the UAV is $\mathbf{h}_d^{\text{H}} \in \mathbb{C}^{1 \times N}$. $\mathbf{G}_{\text{BS}}$ and $\mathbf{G}_k \in \mathbb{C}^{N \times N_r}$ represent the channels from BS_{UAV} and BS_k to UAV_{IRS}, respectively. Moreover, $\boldsymbol{p}_k$ and $\boldsymbol{p}_{\text{BS}} \in \mathbb{C}^{N_r \times 1}$ denote the transmit-power vector of BS_k and BS_{UAV}, respectively. Therefore, the received signal at the UAV is represented as:

$$
\begin{aligned}
y_u \;=\; & \left(\mathbf{h}_{\text{BS}} + \mathbf{h}_d^{\text{H}} \boldsymbol{\Theta} \mathbf{G}_{\text{BS}}\right) \boldsymbol{p}_{\text{BS}} x_{\text{BS}} \\
& + \sum_{k \in \mathcal{S}} \left(\mathbf{h}_k + \mathbf{h}_d^{\text{H}} \boldsymbol{\Theta} \mathbf{G}_k\right) \boldsymbol{p}_k x_k + n_u
\end{aligned}
\tag{2}
$$

where the symbols transmitted by BS_{UAV} and BS_k are respectively denoted as x_{BS}, x_k and $n_u \sim \mathcal{CN}(0, \sigma_u)$ is the additive white Gaussian noise (AWGN) with zero-mean and variance σ_u^2 at the UAV. Therefore, the SINR at the target UAV is given by:

$$
\beta = \frac{|\boldsymbol{\ell}_{\text{BS}} \boldsymbol{p}_{\text{BS}}|^2}{\sum_{k \in \mathcal{S}} |\boldsymbol{\ell}_k \boldsymbol{p}_k|^2 + \sigma_u^2}
\tag{3}
$$

where $\boldsymbol{\ell}_{\text{BS}} = \mathbf{h}_{\text{BS}} + \mathbf{h}_d^{\text{H}} \boldsymbol{\Theta} \mathbf{G}_{\text{BS}}$ and $\boldsymbol{\ell}_k = \mathbf{h}_k + \mathbf{h}_d^{\text{H}} \boldsymbol{\Theta} \mathbf{G}_k$. Obviously, the interference from the co-channels is directly affected by the configuration of IRS meta-atoms. Therefore, choosing α_i and θ_i for each IRS element has a vital role in maximizing β. IRS elements can occasionally function as active components for channel estimation; however, this paper focuses only on passive elements and provides perfect Channel State Information (CSI) which is acquired between the UAV and each BS [13]. This assumption is reasonable due to the strong LoS links between the elevated UAV and ground terminals.

2.2 Problem Definition

With the overwhelming rise of data traffic, data rates, reduced latency and the need for highly reliable and secure communications, network energy consumption poses a significant economic challenge and a major hurdle for next-generation wireless networks. This emphasizes the need for energy-efficient solutions, paving the way for green cellular networks. The objective of this paper is to minimize the required transmit power from the BS_{UAV} by simultaneously optimizing IRS coefficients, $\boldsymbol{\Theta}$. The optimization problem that minimizes the transmit power while ensuring the QoS can be set as follows:

$$
\min_{\boldsymbol{\Theta}} \quad ||\boldsymbol{p}_{\text{BS}}||^2
\tag{4a}
$$

$$
s.t. \quad \beta \geq \gamma
\tag{4b}
$$

$$
\alpha_i \in [0,1], \forall i \in \mathcal{N}
\tag{4c}
$$

$$
\theta_i \in [0, 2\pi), \forall i \in \mathcal{N}
\tag{4d}
$$

$$
\sqrt{(x_{\text{U}}^{t+1} - x_{\text{U}}^t)^2 + (y_{\text{U}}^{t+1} - y_{\text{U}}^t)^2} \leq V_{\max}
\tag{4e}
$$

$$
x_{\min} \leq x_{\text{U}}^t \leq x_{\max}
\tag{4f}
$$

$$
y_{\min} \leq y_{\text{U}}^t \leq y_{\max}
\tag{4g}
$$

where $\{x_{\min}, x_{\max}\}$ and $\{y_{\min}, y_{\max}\}$ denote the boundary of the coordinate of the UAV (or UAV_{IRS}) x_{U} and x_{U}, respectively. (4b) represents the SINR threshold, γ, that ensures the acceptable QoS of UAV. In (4e), it is ensured that the UAV does not exceed its maximum speed. The range of tasks that the UAV can perform is constrained to those specified in (4f) and (4g). We consider that the BS has access to perfect CSI for all links, as explained in [8], to fully assess the capabilities of the IRS. Clearly, the problem in (4) is non-convex due to the left-hand-side of (4b), which is not jointly concave with respect to p_{BS} and $\boldsymbol{\Theta}$.

The challenge in solving (4) arises due to the interdependence between the design variables $\boldsymbol{p}_{\text{BS}}$ and $\boldsymbol{\Theta}$ in (4a)-(4b). To address this, Hua et al. [7] introduced a dual loop AO method based on penalty approaches. This algorithm updates the auxiliary variables by solving a quadratically constrained quadratic program. While the AO approach with a penalty technique achieves variable decoupling, it

suffers from limited solution efficiency. Furthermore, the complexity per iteration of the penalty-based method was $\mathcal{O}(N^3)$. On the other hand, SDR with Gaussian randomization [8] can solve (4). However, the utilization of SDR becomes increasingly complex as the number of meta-atoms grows. Furthermore, obtaining a rank-1 feasible solution necessitates a considerable number of randomization steps, thereby substantially contributing to the overall complexity. Finally, since the coupling between Θ and p_{BS} is high, AO-based methods are typically inefficient, as they can not guarantee a theoretically stationary point.

3. OPTIMAL TRANSMIT POWER USING SCA

In this section, we present a solution to non-convexity of (4b). We address the non-convexity in (4) by using an SCA to produce a high-performance solution. Our approach relies on a set of (in)equalities for arbitrary complex-valued vectors a and b, as described in [35]:

$$||a||^2 \geq 2\Re\{b^{\text{H}}a\} - ||b||^2, \tag{5a}$$

$$\Re\{a^{\text{H}}b\} = \frac{1}{4}(||a+b||^2 - ||a-b||^2), \tag{5b}$$

$$\Im\{a^{\text{H}}b\} = \frac{1}{4}(||a-jb||^2 - ||a+jb||^2) \tag{5c}$$

First, to handle (4b), we employ the method of SCA, where both Θ and p_{BS} are optimized in each iteration. Initially, we use (3) to transform (4b) into an equivalent form given by:

$$\frac{|\ell_{\text{BS}}p_{\text{BS}}|^2}{\gamma} \geq \sum_{k \in \mathcal{S}} |\ell_k p_k|^2 + \sigma_u^2 \tag{6}$$

We observe that the term in (4b) is non-convex. However, since we aim to maximize the right-hand side of (6), we can extract a concave lower bound for it using the following approach:

$$
\begin{aligned}
|\ell_{\text{BS}}p_{\text{BS}}|^2 \;&\overset{(a)}{\geq}\; 2\Re\{(u^{(m)})^{\text{H}}\ell_{\text{BS}}p_{\text{BS}}\} - |u^{(m)}|^2 \\
&\overset{(b)}{\geq}\; \frac{1}{2}\{||u^{(m)}\ell_{\text{BS}}^{\text{H}} + p_{\text{BS}}||^2 \\
&\quad - ||u^{(m)}\ell_{\text{BS}}^{\text{H}} - p_{\text{BS}}||^2\} - |u^{(m)}|^2 \\
&\overset{(c)}{\geq}\; [\,\Re\{(v^{(m)})^{\text{H}}[u^{(m)}\ell_{\text{BS}}^{\text{H}} + p_{\text{BS}}]\,\} - \frac{1}{2}||v^{(m)}||^2 \\
&\quad - \frac{1}{2}||u^{(m)}\ell_{\text{BS}}^{\text{H}} - p_{\text{BS}}||^2 - |u^{(m)}|^2] \\
&= f(p_{\text{BS}};\Theta;p_{\text{BS}}^{(m)};\Theta^{(m)}),
\end{aligned}
\tag{7}
$$

where $u^{(m)} = \ell_{\text{BS}}^{(m)}p_{\text{BS}}^{(m)}$, $v^{(m)} = u^{(m)}(\ell_{\text{BS}}^{(m)})^{\text{H}} + p_{\text{BS}}^{(m)}$ and $\ell_{\text{BS}}^{(m)} = h_{\text{BS}} + h_d^{\text{H}}\Theta^{(m)}h_{\text{BS}}$. Here, $\Theta^{(m)}$ and $\ell_{\text{BS}}^{(m)}$ denote the values of Θ and ℓ_{BS} in the mth iteration of the SCA model, respectively. Additionally, (a) and (c) in (7) result from (5a), while (b) results from (5b). It can be proven that $f(p_{\text{BS}};\Theta;p_{\text{BS}}^{(m)};\Theta^{(m)})$ is jointly concave w.r.t. Θ and p_{BS}.

Next, to address (4b), we utilize the concept of SCA, where we optimize both Θ and p_{BS} in each iteration. Initially, we transform (4b) into an equivalent form as:

$$\frac{|\ell_{\text{BS}}p_{\text{BS}}|^2}{\gamma} \geq \sigma_u^2 + \sum_{k \in \mathcal{S}} (\varrho_k^2 + \bar{\varrho}_k^2), \tag{8a}$$

$$\varrho_k \geq |\Re\{\ell_k p_k\}|, \forall k \in \mathcal{S}, \tag{8b}$$

$$\bar{\varrho}_k \geq |\Im\{\ell_k p_k\}|, \forall k \in \mathcal{S} \tag{8c}$$

where the new slack variables ϱ_k and $\bar{\varrho}_k$ are used. It is simple to observe that if (2.2b) is feasible, then (8) is also feasible and *vice versa*. Since the right-hand side (RHS) of (8a) is convex, we need to find a concave lower bound for the term $|\ell_{\text{BS}}p_{\text{BS}}|^2$ in (8a). Let $p_{\text{BS}}^{(m)}$ and $\Theta^{(m)}$ represent the value of Θ and p_{BS} in the mth iteration of the SCA process, respectively. Similarly to (7), this can be represented as:

$$
\begin{aligned}
\frac{|\ell_{\text{BS}}p_{\text{BS}}|^2}{\gamma} \;&\geq\; \frac{1}{\gamma}[\,\Re\{(v^{(m)})^{\text{H}}[\,u^{(m)}\ell_{\text{BS}}^{\text{H}} - p_{\text{BS}}]\,\} \\
-\frac{1}{2}||v^{(m)}||^2 \;&\quad -\frac{1}{2}||u^{(m)}\ell_{\text{BS}}^{\text{H}} - p_{\text{BS}}||^2 - |u^{(m)}|^2] \\
&= f(p_{\text{BS}};\Theta;p_{\text{BS}}^{(m)};\Theta^{(m)}).
\end{aligned}
\tag{9}
$$

190

Jordanian Journal of Computers and Information Technology (JJCIT), Vol. 11, No. 02, June 2025.

By utilizing the property that $x \geq |y|$ if and only if $x \geq y$ and $x \geq -y$ and incorporating (5b), we can express (8b) in an equivalent form as:

$$\varrho_k \geq \Re\{\boldsymbol{\ell}_k \boldsymbol{p}_k\} = \tfrac{1}{4}(||(\boldsymbol{\ell}_k + \boldsymbol{p}_k||^2 - ||(\boldsymbol{\ell}_k - \boldsymbol{p}_k||^2), \tag{10a}$$

$$\varrho_k \geq -\Re\{\boldsymbol{\ell}_k \boldsymbol{p}_k\} = \tfrac{1}{4}(||(\boldsymbol{\ell}_k - \boldsymbol{p}_k||^2 - ||(\boldsymbol{\ell}_k + \boldsymbol{p}_k||^2) \tag{10b}$$

Due to the presence of the negative quadratic term on the right-hand side of (10a), it becomes non-convex. Therefore, we can transform it into convex by applying the inequality in (5a) as:

$$\varrho_k \geq \tfrac{1}{4}[\left\|\boldsymbol{\ell}_k^{\mathrm{H}} + \boldsymbol{p}_k\right\|^2 - 2\Re\{(\boldsymbol{\ell}_k^{(m)} - (\boldsymbol{p}_k^{(m)})^{\mathrm{H}}(\boldsymbol{\ell}_k^{\mathrm{H}} - \boldsymbol{p}_k)\}$$
$$+ ||(\boldsymbol{\ell}_k^{(m)})^{\mathrm{H}} - \boldsymbol{p}_k^{(m)}||^2] = \rho_k(\boldsymbol{p}_k; \boldsymbol{\Theta}; \boldsymbol{p}_k^{(m)}; \boldsymbol{\Theta}^{(m)}) \tag{11}$$

Applying a similar argument,(10b) results in:

$$\varrho_k \geq \tfrac{1}{4}[\left\|\boldsymbol{\ell}_k^{\mathrm{H}} + \boldsymbol{p}_k\right\|^2 - 2\Re\{(\boldsymbol{\ell}_k^{(m)} + (\boldsymbol{p}_k^{(m)})^{\mathrm{H}}(\boldsymbol{\ell}_k^{\mathrm{H}} + \boldsymbol{p}_k)\}$$
$$+ ||(\boldsymbol{\ell}_k^{(m)})^{\mathrm{H}} + \boldsymbol{p}_k^{(m)}||^2] = \bar{\rho}_k(\boldsymbol{p}_k; \boldsymbol{\Theta}; \boldsymbol{p}_k^{(m)}; \boldsymbol{\Theta}^{(m)}) \tag{12}$$

Similarly, in (11) and (12), (8c) results in the following inequalities:

$$\bar{\varrho}_k \geq \tfrac{1}{4}[||\boldsymbol{\ell}_k^{\mathrm{H}} - j\boldsymbol{p}_k||^2 - 2\Re\{(\boldsymbol{\ell}_k^{(m)} - j(\boldsymbol{p}_k^{(m)})^{\mathrm{H}}(\boldsymbol{\ell}_k^{\mathrm{H}} + j\boldsymbol{p}_k)\}$$
$$+ ||(\boldsymbol{\ell}_k^{(m)})^{\mathrm{H}} + j\boldsymbol{p}_k^{(m)}||^2] = \omega_k(\boldsymbol{p}_k; \boldsymbol{\Theta}; \boldsymbol{p}_k^{(m)}; \boldsymbol{\Theta}^{(m)}) \tag{13}$$

$$\bar{\varrho}_k \geq \tfrac{1}{4}[||\boldsymbol{\ell}_k^{\mathrm{H}} + j\boldsymbol{p}_k||^2 - 2\Re\{(\boldsymbol{\ell}_k^{(m)} + j(\boldsymbol{p}_k^{(m)})^{\mathrm{H}}(\boldsymbol{\ell}_k^{\mathrm{H}} - j\boldsymbol{p}_k)\}$$
$$+ ||(\boldsymbol{\ell}_k^{(m)})^{\mathrm{H}} - j\boldsymbol{p}_k^{(m)}||^2] = \bar{\omega}_k(\boldsymbol{p}_k; \boldsymbol{\Theta}; \boldsymbol{p}_k^{(m)}; \boldsymbol{\Theta}^{(m)}) \tag{14}$$

Subsequently, the only remaining issue is the non-convexity of (4c) and (4d). To tackle this issue, we begin by transforming the equality constraint in (4c) and (4d) into a convex inequality constraint. We introduce a regularization term into the objective function to guarantee the satisfaction of the inequality constraint as an equality at convergence. Additionally, To tackle the non-convexity of the resulting objective function, we employ a first-order approximation of the regularization term centered around $\boldsymbol{\Theta}^{(m)}$. As a result, we can restate the non-convex problem in (4) to approximate the convex sub-problem of the SCA model to an equivalent form as:

$$\min_{\boldsymbol{\Theta},\tau,\bar{\tau}} \quad ||p_{\mathrm{BS}}||^2 - \delta[2\Re\{(\boldsymbol{\Theta}^{(m)})\boldsymbol{\Theta}\} - \|\boldsymbol{\Theta}^{(m)}\|^2], \tag{15a}$$

$$s.t. \quad f(\boldsymbol{p}_{\mathrm{BS}}; \boldsymbol{\Theta}; \boldsymbol{p}_{\mathrm{BS}}^{(m)}; \boldsymbol{\Theta}^{(m)}) \geq \sigma_u^2 + \sum_{k \in \mathcal{S}} (\varrho_k^2 + \bar{\varrho}_k^2), \quad \forall k \in \mathcal{S} \tag{15b}$$

$$(11) - (14), \quad \forall k \in \mathcal{S} \tag{15c}$$

$$\alpha_i \in [0,1], \quad \forall i \in \mathcal{N} \tag{15d}$$

$$\theta_i \in [0,2\pi), \quad \forall i \in \mathcal{N} \tag{15e}$$

where the regularization parameter is defined as $\delta > 0$, m is the iteration number, $\tau = \{\varrho_k\}_{k \in \mathcal{S}}$ and $\bar{\tau} = \{\bar{\varrho}_k\}_{k \in \mathcal{S}}$. Note that the non-convexity of the regularization parameter δ in (15a) leads to the non-convexity of (15). However, to address this issue, we utilize (5a) to convexify (15a). It is evident that all the constraints specified in (15) can be expressed using quadratic cones. Consequently, (15) qualifies as an SOCP problem that can be efficiently solved using the MOSEK solver [36]. When the objective function gradually falls, it eventually reaches a specific threshold ϵ and the optimal $\boldsymbol{\Theta}^\star$ is achieved based on the eigenvalues' decomposition.

4. ALGORITHM ANALYSIS

The proposed algorithm is summarized in Algorithm 1, where the optimization of $\boldsymbol{\Theta}$ aims to minimize the BS transmit power, which is achieved by tuning ϵ using the MOSEK solver. In this section, the feasibility of interference elimination is discussed for LoS channels, then convergence behavior and computational complexity are presented.

4.1 Feasibility of Interference Elimination in LoS Channels

We investigate a special case of pure LoS channels between BS-UAV, UAV$_{\mathrm{IRS}}$-UAV and BS-UAV$_{\mathrm{IRS}}$ to understand the impact of the number of reflecting elements on interference-cancellation feasibility.

This scenario is significant in practical applications owing to the elevated altitude of the UAV and UAV$_{IRS}$. Consequently, we can determine the channel gains for the direct and cascaded paths related to BS$_k$.

Algorithm 1: SCA-based algorithm for solving (15)

Input: Maximum iteration number M, the initial value ($\boldsymbol{p}_{BS}{}^{(0)}$, $\boldsymbol{\Theta}^{(0)}$, $\delta > 0$)

Output: The optimal value $\{\boldsymbol{p}_{BS}{}^*, \boldsymbol{\Theta}^*\}$

Initialize: $m = 0$;

1 repeat

2   The optimal solution of (15) based-MOSEK tool is $\boldsymbol{p}_{BS}{}^{(0)}, \boldsymbol{\Theta}^{(0)}$.

3   Update $\boldsymbol{p}_{BS}{}^{(m+1)} \leftarrow \boldsymbol{p}_{BS}{}^*$, $\boldsymbol{\Theta}^{(m+1)} \leftarrow \boldsymbol{\Theta}^{\star}$

4 $m \leftarrow m+1$

5 until *The objective value of (15) converges*;

$$\|\mathbf{h}_k\|_1 = \frac{\sqrt{\beta_0}}{d_{BU,k}}, k \in \mathcal{S} \tag{16a}$$

$$\left\|\mathbf{h}_d^H \boldsymbol{\Theta} \mathbf{G}_k\right\|_1 = \frac{N\beta_0}{d_{BI,k} d_{IU}}, k \in \mathcal{S} \tag{16b}$$

Here, β_0 represents the LoS path loss at a reference distance of 1 meter. $d_{BU,k}$, d_{IU} and $d_{BI,k}$ denote the distances between the BS$_k$-UAV, UAV$_{IRS}$-UAV and BS$_k$-UAV$_{IRS}$, respectively. Substituting (16a) and (16b) into the complete interference-nulling condition, $\|\mathbf{h}_d^H \boldsymbol{\Theta} \mathbf{G}_k\|_1 \geq \|\mathbf{h}_k\|_1$, we obtain:

$$\frac{N\beta_0}{d_{BI,k} d_{IU}} \geq \frac{\sqrt{\beta_0}}{d_{BU,k}}, k \in \mathcal{S} \tag{17}$$

In this scenario, the elevated altitude of both the UAV and UAV$_{IRS}$ and their close proximity result in approximately equal distances, indicated by $d_{BU,k} \approx d_{BI,k}$. Consequently, we can simplify the expression for the minimum number of reflecting elements required to achieve interference nulling at the UAV as $N_{min} = \left\lceil \frac{d_{IU}}{\sqrt{\beta_0}} \right\rceil$. This suggests that a larger number of reflecting elements facilitates the achievement of interference nulling, as demonstrated through simulations in Section 5.

4.2 Convergence Behavior of Algorithm

Without loss of generality and for a given δ, let $f(\boldsymbol{p}_{BS}{}^{(m)}; \boldsymbol{\Theta}^{(m)})$ be the total transmit power and passive beamforming IRS coefficients' matrix at the mth iteration. Thus, we observe:

$$f(\boldsymbol{p}_{BS}{}^{(m)}; \boldsymbol{\Theta}^{(m)}) \geq f(\boldsymbol{p}_{BS}{}^{(m+1)}; \boldsymbol{\Theta}^{(m)}) \tag{18}$$

where (18) holds since (15) represents a convex function and the transmit power $\boldsymbol{p}_{BS}{}^{(m+1)}$ is optimized and updated at $(m+1)^{th}$ iteration based on the passive beamforming $\boldsymbol{\Theta}^{(m)}$. Interestingly though, $\boldsymbol{p}_{BS}{}^{(m+1)}$ remains unchanged during the $(m+1)^{th}$ iteration, even with the updated passive beamforming $\boldsymbol{\Theta}^{(m+1)}$. Therefore, (18) holds. Considering the constraint (15c), the objective sequence is $f(\boldsymbol{p}_{BS}; \boldsymbol{\Theta}) \geq -\delta M$, indicating that the objective function $f(\boldsymbol{p}_{BS}{}^{(m)}; \boldsymbol{\Theta}^{(m)})$ converges. Also, taking into account the limited system resources and the minimum SINR, we assume that the objective function in (15) must have a lower bound, which is a finite value. Consequently, we can prove the convergence of Algorithm 1 towards a feasible solution.

4.3 Computational-complexity Analysis

Let's suppose that we have only one UAV. It can be easily demonstrated that there are $2(K + N + 1) + 1$ optimization variables in total in (15), considering that they are real-valued. There are $N + 2$ total second-order conic restrictions. As a result, using the justifications in [37], the suggested SOCP-based method's overall per-iteration complexity is given by:
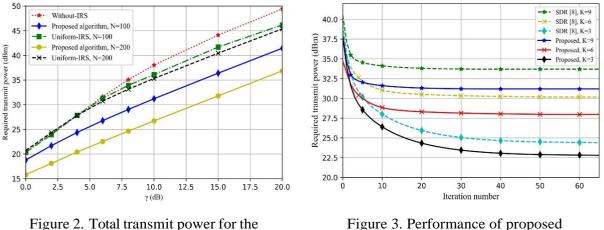
$$\mathcal{O}[2(4 + N)^{0.5}(1 + K + N)(4 + 16K + 8N + 20K^2 + 8KL + 4N^2)] \tag{19}$$

In realistic scenarios, the IRS meta-atoms are anticipated to be significantly greater than the number of interfering BSs. Consequently, the complexity of Algorithm 1-based SCA can be accurately

192

Jordanian Journal of Computers and Information Technology (JJCIT), Vol. 11, No. 02, June 2025.

approximated as $\mathcal{O}(N^{3.5})$. Although the use of AO in [7] simplifies the optimization problem, the complex interdependence among the design variables may prevent it from producing a solution of high quality. Furthermore, as demonstrated in Section 5, employing a penalty-based algorithm necessitates a substantial number of iterations to meet convergence, resulting in prolonged problem-solving time. On the other hand, the complexity of the SDR-based algorithm discussed in [8] is dominated by solving the semi-definite program (SDP) in (8), resulting in a per-iteration complexity of approximately $\mathcal{O}(N^7)$ [37]. This is significantly higher than the complexity of our proposed algorithm, especially for large numbers of IRS meta-atoms. As we will demonstrate numerically in the next section, our algorithm offers significant computational advantages.

5. NUMERICAL RESULTS

This section documents numerical results that demonstrate the performance of Algorithm 1. For the simulation, we examine a system that incorporates an IRS to assist a UAV, where the BS_{UAV} and UAV_{IRS} are positioned at (0, 0, 10 m) and $(x_{\text{U}}, y_{\text{U}}, 50\ m)$, respectively. The remaining co-channel BSs are situated at 10 m height, the locations are randomly and uniformly generated within their respective cells, which are denoted by coordinates $(x_{\text{BS},k}, y_{\text{BS},k}, 10\ m)$. The UAV_{IRS} operates at a constant altitude h_{U}, with a flight duration T set to 80 seconds and the maximum speed of the UAV is $V_{\text{max}} = 25\ m/s$. With a total bandwidth of 10 MHz, we suppose that the system operates at its center frequency of 2.4 GHz. Additionally, we consider parameters $\delta = 0.001$ and $\sigma^2 = -174$ dBm. The UAV-UAV_{IRS} channel is assumed to exhibit Rayleigh fading, whereas the BS-UAV channels are modeled using Rician fading with a Rician factor of K=5 and distance-dependent path-loss for the communication links, as described in [38].

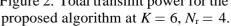Figure 2. Total transmit power for the proposed algorithm at $K = 6$, $N_{\text{r}} = 4$.

Figure 3. Performance of proposed algorithm at different K values and N=200.

Fig. 2 quantifies the relationship between the transmit power and threshold SINR with $K = 6$, where the effect of Algorithm 1 is shown with varying numbers of IRS meta-atoms. In this figure, we calculate the required transmit power without IRS (*i.e.*, $\mathbf{\Theta} = 0$) and compare the result with uniform IRS (*i.e.*, $\mathbf{\Theta} = 1$) at different values of N. We observe that the uniform IRS demonstrates limited effectiveness when the threshold SINR falls below 5 dBm, while uniform IRS enhances the received signal for higher γ. Its impact is not substantial enough to overcome the interference signals introduced by the BS when the SINR threshold is below 5 dBm. Consequently, the required transmit power is decreased by increasing the number of IRS meta-atoms. Moreover, Fig. 2 shows the required transmit power for Algorithm 1 and compares it with the uniform IRS at $N = 100$ and $N = 200$. We notice that the required transmit power for Algorithm 1 is less than the required power for uniform IRS. For example, when $\gamma = 10$ dB, the required transmit power for Algorithm 1 at $N = 100$ is approximately 5 dBm less than that of the uniform IRS. Similarly, when $N = 200$, the reduction is approximately 13 dBm. These results emphasize the advantage of the IRS-aided communication system, enabling the UAV to achieve reduced required transmit power while maintaining the desired QoS and SINR level. Additionally, it shows the savings in power when utilizing the proposed algorithm.

"Towards Optimizing the Downlink Transmit Power in UAV-Integrated IRS Wireless Systems", A. Reda, T. Mekkawy and A. Mahran.

Figure 3 illustrates the performance of Algorithm 1 compared to the SDR-based approach [8] using a predefined threshold of $\gamma = 10$ and $N_r = 4$. Through comparisons involving varying numbers of interference base stations while maintaining the same number of IRS meta-atoms (*i.e.*, $K = 3$, $K = 6$ and $K = 9$ with $N = 200$), it is observed that the necessary transmit power increases with a rise in the number of interference base stations. The figure distinctly shows that Algorithm 1 surpasses the SDR-based algorithm in terms of the required transmit power. Additionally, this effect is attributed to the destructive beam effects towards the primary network, which satisfies constraint (4b) and consequently reduces interference, resulting in an improved required transmit power.

The convergence analysis of Algorithm 1 is illustrated in Figure 4. We use different initial values for Θ_i, uniform ($\Theta = 1$), randomly distributed (Θ with randomized θ and α), or $\Theta = 0$. The convergence is shown for $K = 6$, $N = 100$, $N_r = 4$ and two values for γ. We observe the rapid convergence of the proposed algorithm reaching its convergence point within the 8th iteration for any initial point. Also, we show that the required transmit power is increased by increasing the threshold value of γ. In other words, increasing the QoS for the UAV requires more base station's transmit power.
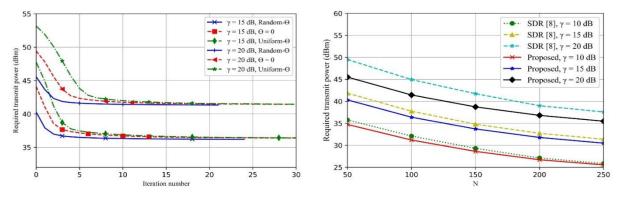

Figure 4. Convergence behavior of Algorithm 1 (N=100).

Figure 5. Total required transmit power *versus* SCA-IRS meta-atoms for K=6 and Nr=4 under different schemes.

Figure 5 illustrates the relationship between the required transmit power and the number of IRS meta-atoms for various threshold SINR values, considering the calculated optimal IRS coefficient Θ. Additionally, the performance of the SDR-based method [8] is presented. As anticipated, a decreasing trend in the necessary transmit power is observed with an increasing number of IRS meta-atoms. This trend can be attributed to the passive nature of the IRS, where a higher count of phase shifters allows for more power to be reflected from the BS. Consequently, this amplifies the SINR, resulting in a reduced required transmit power. Both the transmit power of BS_{UAV} and that of each co-channel BS_k are set to be equal, denoted as $\boldsymbol{p}_{BS} = \boldsymbol{p}_k$ [13]. It is important to note that the required transmit power of the UAV to achieve a specific SINR and the received interference power exhibit a steady increase or decrease with N. However, as N increases, the UAV transmit power decreases due to substantial interference suppression by the IRS, leading to a more prominent desired signal power. Furthermore, the figure indicates that the SDR-based methods exhibit similar performance for small values of γ. Conversely, for larger γ, Algorithm 1 outperforms the SDR-based methods.
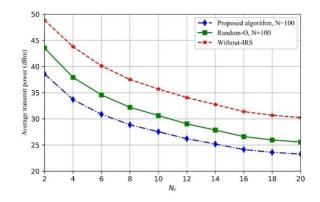

Figure 6. Transmit power of the BS *versus* number of antennas at BS_{UAV}.

Finally, Figure 6 illustrates the anticipated decrease in average transmit power required for information transmission as the number of transmit antennas at the BS_{UAV} increases for $\gamma = 10$ and $K = 6$. This effect is attributed to the availability of more DoF for spatial multiplexing with a larger antenna array, allowing for lower transmit at the BS. Furthermore, it can be observed that employing phase shifts at the IRS yields significant performance gains compared to random phase or the absence of IRS. These findings highlight the effectiveness of multiple-antenna techniques in reducing transmit power.

6. CONCLUSIONS

In this paper, we have presented a framework that leverages the SCA algorithm and SOCP relaxation to optimize both the phase-shift and amplitude coefficients of the IRS matrix. This approach effectively addresses the challenge of minimizing transmit power for UAV-downlink communication while maintaining QoS. Notably, the algorithm updates all optimization variables simultaneously in each iteration, ensuring efficient convergence. Furthermore, we investigate the impact of exploiting both the direct channel and the reflected signal from the IRS, enabling constructive interference and enhanced reception at the target UAV. The combined use of SOCP and SCA facilitates rapid convergence to an effective solution. Simulations demonstrate that our IRS-aided UAV communication system achieves significant power savings of approximately 13 dBm compared to conventional approaches while maintaining the desired SINR level across various interference scenarios. In our future work, we aim to address the challenge of analyzing how altitude and speed impact interference mitigation. Additionally, we will explore the challenges of dynamic channel conditions and imperfect CSI.

REFERENCES

[1] Y. Zeng, Q. Wu and R. Zhang, "Accessing from the Sky: A Tutorial on UAV Communications for 5G and beyond," Proceedings of the IEEE, vol. 107, no. 12, pp. 2327–2375, 2019.

[2] A.-A. A. Boulogeorgos and A. Alexiou, "Coverage Analysis of Reconfigurable Intelligent Surface Assisted THz Wireless Systems," IEEE Open J. of Vehicular Technology, vol. 2, pp. 94–110, 2021.

[3] A. Ihsan, W. Chen, M. Asif, W. U. Khan, Q. Wu and J. Li, "Energy-efficient IRS-aided NOMA Beamforming for 6G Wireless Communications," IEEE Transactions on Green Communications and Networking, vol. 6, no. 4, pp. 1945–1956, 2022.

[4] Q. Wu, S. Zhang, B. Zheng, C. You and R. Zhang, "Intelligent Reflecting Surface-aided Wireless Communications: A Tutorial," IEEE Trans. on Communications, vol. 69, no. 5, pp. 3313–3351, 2021.

[5] T. Song, D. Lopez, M. Meo, N. Piovesan and D. Renga, "High Altitude Platform Stations: The New Network Energy Efficiency Enabler in the 6G Era," Proc. of the 2024 IEEE Wireless Communications and Networking Conference (WCNC), pp. 1–6, Dubai, UAE, 2024.

[6] S. Khisa, M. Elhattab, C. Assi and S. Sharafeddine, "Energy Consumption Optimization in RIS-assisted Cooperative RSMA Cellular Networks," IEEE Trans. on Communications, vol. 71, no. 7, pp. 4300–4312, 2023.

[7] M. Hua, Q. Wu, W. Chen, O. A. Dobre and A. Lee Swindlehurst, "Secure Intelligent Reflecting Surface Aided Integrated Sensing and Communication," IEEE Trans. on Wireless Communications, vol. 23, no. 1, pp. 575–591, 2023.

[8] Q. Wu and R. Zhang, "Intelligent Reflecting Surface Enhanced Wireless Network *via* Joint Active and Passive Beamforming," IEEE Trans. on Wireless Communi., vol. 18, no. 11, pp. 5394–5409, 2019.

[9] M. A. ElMossallamy, K. G. Seddik, W. Chen, L. Wang, G. Y. Li and Z. Han, "RIS Optimization on the Complex Circle Manifold for Interference Mitigation in Interference Channels," IEEE Transactions on Vehicular Technology, vol. 70, no. 6, pp. 6184–6189, 2021.

[10] M. Cui, G. Zhang and R. Zhang, "Secure Wireless Communication via Intelligent Reflecting Surface," IEEE Wireless Communications Letters, vol. 8, no. 5, pp. 1410–1414, 2019.

[11] H. Niu, Z. Chu, F. Zhou and Z. Zhu, "Simultaneous Transmission and Reflection Reconfigurable Intelligent Surface-assisted Secrecy MISO Networks," IEEE Communications Letters, vol. 25, no. 11, pp. 3498–3502, 2021.

[12] Y. Liu, J. Yang, K. Huang, X. Sun and Y. Wang, "Secure Wireless Communications in the Multi-user MISO Interference Channel Assisted by Multiple Reconfigurable Intelligent Surfaces," Journal of Communications and Networks, vol. 24, no. 5, pp. 530–540, 2022.

[13]   X. Pang, W. Mei, N. Zhao and R. Zhang, "Intelligent Reflecting Surface-assisted Interference Mitigation for Cellular-connected UAV," IEEE Wireless Communications Letters, vol. 11, no. 8, pp. 1708–1712, 2022.

[14]   X. Wu, J. Ma, Z. Xing, C. Gu, X. Xue and X. Zeng, "Secure and Energy Efficient Transmission for IRS-assisted Cognitive Radio Networks," IEEE Trans. on Cognitive Communications and Networking, vol. 8, no. 1, pp. 170–185, 2022.

[15]   M. Kim and D. Park, "Intelligent Reflecting Surface-aided MIMO Secrecy Rate Maximization," ICT Express, vol. 8, no. 4, pp. 518–524, 2022.

[16]   W. Jiang, Y. Zhang, J. Zhao, Z. Xiong and Z. Ding, "Joint Transmit Precoding and Reflect Beamforming Design for IRS-assisted MIMO Cognitive Radio Systems," IEEE Transactions on Wireless Communications, vol. 21, no. 6, pp. 3617–3631, 2022.

[17]   V. Kumar, M. Chafii, A. L. Swindlehurst, L.-N. Tran and M. F. Flanagan, "SCA-based Beamforming Optimization for IRS-enabled Secure Integrated Sensing and Communication," arXiv preprint, arXiv: 2305.03831, 2023.

[18]   P. Liu, G. Jing, H. Liu, L. Yang and T. A. Tsiftsis, "Intelligent Reflecting Surface-assisted Cognitive Radio-inspired Rate-splitting Multiple Access Systems," Digital Communications and Networks, vol. 9, no. 3, pp. 655–666, 2023.

[19]   J. Ye, S. Guo and M.-S. Alouini, "Joint Reflecting and Precoding Designs for SER Minimization in Reconfigurable Intelligent Surfaces-assisted MIMO Systems," IEEE Trans. Wireless Commun., vol. 19, no. 8, pp. 5561–5574, 2020.

[20]   Z. Albataineh, K. F. Hayajneh, H. Shakhatreh, R. A. Athamneh and M. Anan, "Channel Estimation for Reconfigurable Intelligent Surface-assisted mmWave based on Re'nyi Entropy Function," Scientific Reports, vol. 12, no. 1, p. 22301, 2022.

[21]   Q. Wu and R. Zhang, "Beamforming Optimization for Wireless Network Aided by Intelligent Reflecting Surface with Discrete Phase Shifts," IEEE Trans. on Communications, vol. 68, no. 3, pp. 1838–1851, 2020.

[22]   H. Wang, Z. Shi, Y. Fu and R. Song, "Downlink Multi-IRS Aided NOMA System with Second-order Reflection," IEEE Wireless Communications Letters, vol. 12, no. 6, pp. 1022–1026, 2023.

[23]   J. Wang and H. Yu, "Rf Energy Harvesting Schemes for Intelligent Reflecting Surface-aided Cognitive Radio Sensor Networks," Scientific Reports, vol. 12, no. 1, p. 22462, 2022.

[24]   Q.-U.-A. Nadeem, A. Kammoun, A. Chaaban, M. Debbah and M.-S. Alouini, "Asymptotic Max-min SINR Analysis of Reconfigurable Intelligent Surface Assisted MISO Systems," IEEE Trans. on Wireless Communications, vol. 19, no. 12, pp. 7748–7764, 2020.

[25]   W. Feng, J. Tang, Q. Wu, Y. Fu, X. Zhang, D. K. C. So and K.-K. Wong, "Resource Allocation for Power Minimization in RIS-assisted Multi-UAV Networks with NOMA," IEEE Trans. on Communications, vol. 71, no. 11, pp. 6662–6676, 2023.

[26]   H. Wang, C. Liu, Z. Shi, Y. Fu and R. Song, "On Power Minimization for IRS-aided Downlink NOMA Systems," IEEE Wireless on Communications Letters, vol. 9, no. 11, pp. 1808–1811, 2020.

[27]   Y. Cai, Z. Wei, S. Hu, D. W. K. Ng and J. Yuan, "Resource Allocation for Power-efficient IRS-assisted UAV Communications," Proc. of the 2020 IEEE Int. Conf. on Communications Workshops (ICC Workshops), pp. 1–7, Dublin, Ireland, 2020.

[28]   H. Huang, Y. Zhang, H. Zhang, Z. Zhao, C. Zhang and Z. Han, "Multi-IRS-aided Millimeter-wave Multi-user MISO Systems for Power Minimization Using Generalized Benders Decomposition," IEEE Trans. on Wireless Communications, vol. 22, no. 11, pp. 7873–7886, 2023.

[29]   B. Zheng and R. Zhang, "Intelligent Reflecting Surface-enhanced OFDM: Channel Estimation and Reflection Optimization," IEEE Wireless on Communications Letters, vol. 9, no. 4, pp. 518–522, 2020.

[30]   Z. Ji, W. Yang, X. Guan, X. Zhao, G. Li and Q. Wu, "Trajectory and Transmit Power Optimization for IRS-assisted UAV Communication under Malicious Jamming," IEEE Trans. on Vehicular Technology, vol. 71, no. 10, pp. 11262–11266, 2022.

[31]   C. You, Z. Kang, Y. Zeng and R. Zhang, "Enabling Smart Reflection in Integrated Air-Ground Wireless Network: IRS Meets UAV," IEEE Wireless Communications, vol. 28, no. 6, pp. 138–144, 2021.

[32]   A. Khalili, E. M. Monfared, S. Zargari, M. R. Javan, N. M. Yamchi and E. A. Jorswieck, "Resource Management for Transmit Power Minimization in UAV-assisted RIS Hetnets Supported by Dual Connectivity," IEEE Trans. on Wireless Communications, vol. 21, no. 3, pp. 1806–1822, 2022.

[33]   K. Ntontin et al., "Autonomous Reconfigurable Intelligent Surfaces through Wireless Energy

196

Jordanian Journal of Computers and Information Technology (JJCIT), Vol. 11, No. 02, June 2025.

Harvesting," 2022 IEEE 95th Vehicular Technology Conference: (VTC2022-Spring), pp. 1–6, Helsinki, Finland, 2022.

[34] X. Shao and R. Zhang, "Target-mounted Intelligent Reflecting Surface for Secure Wireless Sensing," IEEE Trans. on Wireless Communications, vol. 23, no. 8, pp. 9745–9758, 2024.

[35] V. Kumar, R. Zhang, M. D. Renzo and L.-N. Tran, "A Novel SCA-based Method for Beamforming Optimization in IRS/RIS-assisted MU-MISO Downlink," IEEE Wireless Communications Letters, vol. 12, no. 2, pp. 297–301, 2023.

[36] M. Aps, "Mosek Fusion API for Python 10.0.46," [Online], Available: https://docs.mosek.com/10.0/pythonfusion.pdf.

[37] A. Ben-Tal and A. Nemirovski, Lectures on Modern Convex Optimization: Analysis, Algorithms and Engineering Applications, SIAM Publications Library, 2001.

[38] N. S. Perović, L.-N. Tran, M. Di Renzo and M. F. Flanagan, "On the Maximum Achievable Sum-rate of the RIS-aided MIMO Broadcast Channel," IEEE Trans. on Signal Processing, vol. 70, pp. 6316–6331, 2022.

ملخص البحث:

إنّ التَّداخل بـين الجـوّ والأرض يشـكّل تحـدّياً فـي تحقيـق التّكامـل بـين المركبـات الجوّيـة غيـر المأهولـة وشـبكات الاتّصـالات. ويمكـن للمركبـات الجوّيـة غيـر المأهولـة أن تقـاوم قـدْراً كبيـراً مـن التَّداخل مـن المحطّـات الأرضـية إذا تـمّ ضـمان خـطّ نظـرٍ مباشـر يـربط بينهـا وبـين المسـتخدمين علـى الأرض. لـذا تهـدف هـذه الدّراسـة إلـى التَّركيـز علـى تحسـين القُـدرة فـي المحطّـات الأرضـية وتطبيـق مبـادىء الطّاقـة الخضـراء لتمهيـد الطّريـق نحـو محطّـات أرضـية أكثـر اسـتدامةً وفعاليـة مـن حيـث الطّاقـة فـي أنظمـة الاتّصـال اللاسـلكية المتكاملـة مـع المركبـات الجوّيـة المأهولـة. كمـا تبحـث هـذه الدّراسـة فـي تحسـين قُـدرة الإرسـال فـي رابـط التنزيـل فـي أنظمـة السّـطح العـاكس الـذّكي اللاسـلكية المتكاملـة مـع الطّـائرات بـدون طيّـار؛ إذ يـتمّ تركيـب السّـطح العـاكس الـذّكي علـى الطّـائرة بـدون طيّـار مـن أجـل إزالـة التَّداخل الصّـادر مـن المحطّـات الأرضـية التّابعـة للشّـبكة ذاتها.

وتبـين نتـائج المحاكـاة أنّ النّظـام المقتـرح فـي هـذه الدّراسـة هـو نظـام ذو فاعليـة كبيـرة مـن حيـث تحسـين قـدرة الأرسـال، إلـى جانـب قـدْرٍ مـنخفض مـن تعقيـد الحسـابات، وأداءٍ قريـب مـن المثاليـة يتفـوّق إلـى حـدٍّ كبيـرٍ علـى الأنظمـة التّقليديـة الّتـي تخْلـو مـن أنظمـة السّـطح العـاكس الـذّكي. وتُحقّـق الخوارزميّـة المسـتخدمة خفْضـاً فـي القـدرة يتـراوح بـين 8 و 13 ديسـيبل (dBm)، مـع الحفـاظ علـى نسـبة الإشـارة إلـى التَّداخل والضّـجيج المطلوبة.